Static and thermodynamic properties of low-density supercritical ^{4}He—breakdown of the Feynman–Hibbs approximation†

Piotr Kowalczyk,*[a] Lorenzo Brualla,[b] Piotr A. Gauden[c] and Artur P. Terzyk[c]

Received 8th April 2009, Accepted 17th July 2009
First published as an Advance Article on the web 14th August 2009
DOI: 10.1039/b907165b

We study the applicability of the semiclassical Feynman and Hibbs (FH) (second-order or fourth-order) effective potentials to the description of the thermodynamic properties of quantum fluids at finite temperatures. First, we use path integral Monte Carlo (PIMC) simulations to estimate the thermodynamic/static properties of our model quantum fluid, *i.e.* low-density ^{4}He at 10 K. With PIMC we obtain the experimental equation of state, the single-particle mean kinetic energy, the single-particle density matrix and the single-particle momentum distribution of this system at low densities. We show that our PIMC results are in full agreement with experimental data obtained with deep inelastic neutron scattering at high momentum transfers (D. Colognesi, C. Andreani, R. Senesi, *Europhys. Lett.*, 2000, **50**, 202). As expected, in this region of the ^{4}He phase diagram, quantum effects modify the width of the single-particle momentum distribution but do not alter its Gaussian shape. Knowing the exact values of density, pressure and single-particle mean kinetic energy for our model quantum fluid, we investigate the limitations of the semiclassical FH effective potentials. We show that commonly used 'short-time' approximations to the high-temperature density matrix due to Feynman and Hibbs can only be applied in a very limited range of the ^{4}He phase diagram. We found that FH effective potentials reproduce the experimental densities of ^{4}He at 10 K for $\Lambda/a < 0.45$ ($\Lambda = 2.73$ Å denotes the thermal de Broglie wavelength, $a = \rho^{-1/3}$ is the mean nearest-neighbor distance in the fluid and ρ denotes fluid density). Moreover, semiclassical FH effective potentials are able to correctly predict the single-particle mean kinetic energy of ^{4}He at 10 K in a very limited range of fluid densities, *i.e.* $\Lambda/a < 0.17$. We show that the *ad hoc* application of the semiclassical FH effective potentials for the calculation of the thermodynamic properties of dense liquid-like *para*-hydrogen (*para*-H_2) adsorbed in nanoporous materials below 72 K is questionable.

I. Introduction

There has been tremendous interest in the storage of quantum fluids, particularly molecular hydrogen, in nanoporous materials at finite temperatures.[1–6] Moreover, nanoporous membranes have been suggested as potential quantum filters for efficient separation of hydrogen isotopes at cryogenic temperatures.[7–10] Nevertheless, the correct description of the static and thermodynamic properties of low-dimensional quantum fluids (*i.e.* quantum fluids adsorbed in pores of molecular sizes) is challenging and interesting from the point of view of fundamental physics. In a series of papers, both second- and fourth-order semiclassical FH 'short-time' approximations to the high-temperature density matrix have been recently used for the *ad hoc* description of thermodynamic and transport properties of dense quantum fluids adsorbed in nanoporous materials, for example, H_2 adsorbed in metal–organic frameworks at 40 K,[11] molecular hydrogen and deuterium adsorbed in zeolite Rho II at temperatures down to 30–40 K,[12,13] *etc.* Clearly, semiclassical FH effective potentials are only approximations to the high-temperature density matrix. Thus, the limitations of these semiclassical methods used for simulation of quantum fluids at finite temperatures are important from both theoretical and practical points of view. According to Sesé's[14,15] path integral Monte Carlo (PIMC) studies, the second-order FH effective potential can be used when the reduced de Broglie thermal wavelength, $\Lambda^* \equiv h/(2\pi m k_B T \sigma^2)^{1/2} \leq 0.5$ (here, m denotes the mass of the quantum particle, k_B is the Boltzmann constant, T denotes temperature and σ is the collision diameter of the quantum particle). Note that Λ^* is a function of temperature but not of the bulk or confined quantum fluid density. For ^{4}He at 10.2 K, $\Lambda^* = 1.07$ (*i.e.*, $\Lambda \cong \sigma$), and one can expect that semiclassical FH effective potentials cannot be applied for the calculation of

[a] *Applied Physics, RMIT University, GPO Box 2476V, Victoria, 3001, Australia. E-mail: piotr.kowalczyk@rmit.edu.au; Fax: +61 (0)3 9925 5290; Tel: +61 (0)3 9925 2571*
[b] *Universitat de Barcelona, Facultat de Física (ECM), Diagonal 647, 08028, Barcelona, Spain*
[c] *Department of Chemistry, Physicochemistry of Carbon Materials Research Group, N. Copernicus University, Gagarin St. 7, 87-100, Torun, Poland*

† Electronic supplementary information (ESI) available: Movie 1: delocalization of low-density helium atoms at 10.2 K; movie 2: snapshots of helium at 0.48 MPa and 10.2 K. Marked green helium atom is used for calculation of the momentum distribution; movie 3: snapshots of helium at 1.41 MPa and 10.2 K. Marked green helium atom is used for calculation of the momentum distribution; movie 4: snapshots of helium at 2.46 MPa and 10.2 K. Marked green helium atom is used for calculation of the momentum distribution. See DOI: 10.1039/b907165b

the static and thermodynamic properties of this fluid. Clearly, this assumption is incorrect since quantum effects depend on the fluid density, *i.e.* Λ/a (ratio of the thermal de Broglie wavelength to the mean nearest-neighbor distance in the fluid). To investigate the limitations of the semiclassical FH effective potentials, we combine Feynman's path integral method with experimental data of low-density ^{4}He at 10.2 K.

Of all quantum liquids, ^{4}He is the most common and characteristic one.[16,17] It is, therefore, an ideal system for investigating the microscopic origin of quantum effects and for doing comparisons between experiments and theory.[17–20] Regarding static properties, Ceperley *et al.*,[21] Brualla *et al.*[22] and Mazzanti *et al.*[23] showed that the single-particle momentum distribution of liquid ^{4}He (for clarity, throughout the article we omit the term 'single-particle') deviates from the Gaussian one at sufficiently low temperatures. This effect has been studied using PIMC simulations. The kinetic energy of low temperature liquids cannot be predicted using the Maxwellian kinetic theory of gases, since the kinetic energy is the second moment of the momentum distribution and in the Maxwellian theory this distribution is assumed to be Gaussian. It has been shown that the kinetic energy of liquid ^{4}He is always greater than $3k_BT/2$ (k_B denotes Boltzmann constant and T is the measured temperature) because of the confining effects of the hard cores.

Static and thermodynamic properties of supercritical ^{4}He at low densities have received less attention in comparison to normal or superfluid phases. In relation to supercritical ^{4}He, it is worth mentioning the work of Colognesi *et al.*,[24] in which they experimentally determined the kinetic energy of ^{4}He along two low-density isochores ($\rho = 10.35$ nm^{-3} and $\rho = 13.8$ nm^{-3}) in the temperature range between 5 and 30 K. They concluded that supercritical ^{4}He retains its quantum character even at very low densities.

In the current work, we study the applicability of the semiclassical FH (second-order or fourth-order) effective potentials to the description of the thermodynamic properties of quantum fluids at finite temperatures. We want to underline that we treated low-density ^{4}He at 10 K as a well-known, model quantum fluid. Thus, as we show later, our simulation results can be applicable for any other quantum fluids of industrial importance (*i.e.* molecular hydrogen, neon, xenon and others). From PIMC simulations, we determine the equation of state, the mean kinetic energy, the density matrix and the momentum distribution of ^{4}He at 10 K and pressures up to 2.5 MPa (equivalent bulk density of ^{4}He up to 30 mmol cm^{-3}). We show that PIMC simulations predict a linear increase in the mean kinetic energy with the density in the studied regime. Moreover, the predicted mean kinetic energy of low-density ^{4}He at 10 K is in excellent agreement with the experiment mentioned above, where the results were obtained from deep inelastic neutron scattering experiments at high momentum transfer.[24] Knowing the exact values of density, pressure and mean kinetic energy for our model quantum fluid, we investigate the limitations of the semiclassical FH approximations to the high-temperature density matrix. We found that semiclassical FH effective potentials reproduce the experimental densities of ^{4}He at 10 K for $\Lambda/a < 0.45$. Furthermore, FH effective potentials are able to reproduce the mean kinetic energy of studied ^{4}He only in a very limited range of fluid densities, *i.e.* $\Lambda/a < 0.17$. The density of *para*-H_2 adsorbed in carbon nanotubes and other nanoporous materials at cryogenic temperatures reached 50 mmol cm^{-3} (see ref. 10). In the current study, we predict that FH effective potentials give reliable estimations of *para*-H_2 density at temperatures greater than 72 K (*i.e.* $\Lambda/a < 0.45$), whereas to reproduce the mean kinetic energy of dense liquid-like *para*-H_2, the temperatures should exceed 510 K (*i.e.* $\Lambda/a < 0.17$). This simple example lightly shows the limitations of the semiclassical FH effective potentials.

II. Computational details

II.1 Path integral Monte Carlo simulation

We performed all PIMC simulations in the canonical ensemble. In the path integral formalism, each atom is mapped onto an equivalent polymer chain or 'necklace' of P classical 'beads' $\boldsymbol{r}_i^{(1)}$, $\boldsymbol{r}_i^{(2)}$,..., $\boldsymbol{r}_i^{(P)}$.[25–27] The vector $\boldsymbol{r}$ denotes the position of a bead belonging to the ith atom. In our simulations we have used the primitive action, given by ref. 14, 15 and 27,

$$W = \frac{mP}{2\beta^2\hbar^2}\sum_{i=1}^{N}\sum_{\alpha=1}^{P}(\boldsymbol{r}_i^{(\alpha)} - \boldsymbol{r}_i^{(\alpha+1)})^2 + \frac{1}{P}\sum_{i<j}\sum_{\alpha=1}^{P}V(\boldsymbol{r}_{ij}^{(\alpha)}), \quad (1)$$

where N is the number of atoms, $\beta = (k_BT)^{-1}$ is the inverse of the temperature and $\hbar$ is Planck's constant divided by 2π. Owing to the cyclic condition of the polymer chains, if $\alpha = P$, then $\alpha + 1 = 1$. The interaction potential between helium atoms, $V(r)$, is HFD-B2 He(4), taken from Aziz *et al.*[28] We found that for low-density ^{4}He at 10 K the necessary number of beads per atom was 32 in order to correctly reproduce the experimental equation of state and the mean kinetic energy (see Fig. 1). The temperature that we study is above the λ temperature, and thus exchange effects may be neglected (see ref. 29–36).

The mean kinetic energy has been estimated using the virial estimator given by ref. 21–23,

$$K = \frac{3}{2}T + \frac{1}{2PN}\sum_{i=1}^{N}\sum_{\alpha=1}^{P}(\boldsymbol{r}_i^{(\alpha)} - \boldsymbol{R}_{CM,i})\cdot\frac{\partial V(r_i^{(\alpha)})}{\partial \boldsymbol{r}_i^{(\alpha)}} \quad (2)$$

where $\boldsymbol{R}_{CM,i}$ denotes the centroid position of the ith closed polymer chain.

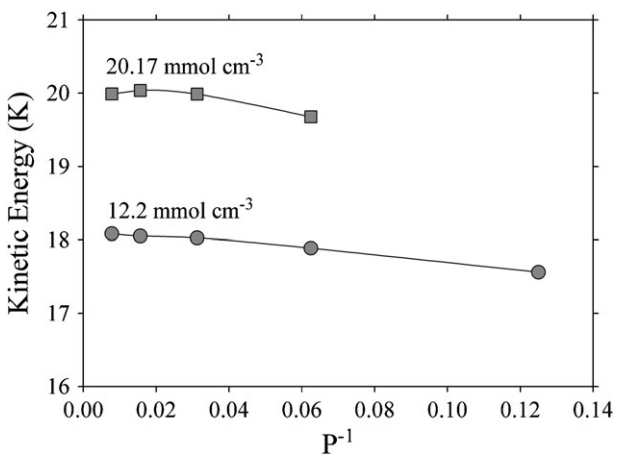

Fig. 1 Variation of the kinetic energy of ^{4}He, quantized by different numbers of beads. Note that for low-density ^{4}He at 10 K, the virial estimator for kinetic energy converges as $P = 32$.

On the other hand, the single particle density matrix is defined as[21]

$$n(\boldsymbol{r}) = Z^{-1} \int \mathrm{d}\boldsymbol{r}_1 \mathrm{d}\boldsymbol{r}_2 \ldots \mathrm{d}\boldsymbol{r}_P \langle \boldsymbol{r}_1, \boldsymbol{r}_2, \ldots, \boldsymbol{r}_P | \exp(-\beta H) | \boldsymbol{r}_1 + \boldsymbol{r}, \boldsymbol{r}_2 + \boldsymbol{r}, \ldots, \boldsymbol{r}_P + \boldsymbol{r} \rangle \quad (3)$$

where Z denotes the partition function and H is the Hamiltonian of the system. From eqn (3), we notice that the off-diagonal part of the density matrix is required. In the polymer isomorphism language, off-diagonal terms imply open chains. We achieved an efficient sampling of the density matrix using the 'trail method' introduced by Brualla *et al.*[21]

The single-particle momentum distribution is defined as the Fourier transform of the single-particle density matrix,[21–23]

$$n(\boldsymbol{k}) = \frac{1}{(2\pi)^3 \rho} \int \exp(-i\boldsymbol{k} \cdot \boldsymbol{r}) n(\boldsymbol{r}) \mathrm{d}\boldsymbol{r} \quad (4)$$

where ρ is the density of the system and $\boldsymbol{k}$ is the reciprocal lattice vector. The normalization of the momentum distribution is given by $\int \mathrm{d}^3\boldsymbol{k} n(\boldsymbol{k}) = 1$. Within the framework of information exchange with experimentalists, the Compton profile becomes relevant, being the observable measured in neutron scattering experiments. At sufficiently high momentum transfer, the impulse approximation holds because the neutron scatters from single atoms. Under the impulse approximation, the Compton profile is defined in terms of the momentum distribution as,[21–23]

$$J_{\mathrm{IA}}(Y) = \frac{1}{4\pi^2 \rho} \int_{|Y|}^{\infty} \boldsymbol{k} n(\boldsymbol{k}) \mathrm{d}\boldsymbol{k} \quad (5)$$

with

$$Y = \frac{m}{q} \left(\omega - \frac{q^2}{2m} \right) \quad (6)$$

where q and ω are the momentum and energy transferred from the neutron to the sample and m denotes the mass of a ^{4}He atom. In PIMC simulations, the single-particle Compton profile is obtained by integration of the single-particle momentum distribution.

In order to see how quantum fluctuations affect both the momentum distribution and the Compton profile, we compared PIMC results with predictions from the classical Maxwellian theory. The classical momentum distribution is given by ref. 21–23,

$$n_C(\boldsymbol{k}) = A \exp\left(-\frac{\lambda}{T} \boldsymbol{k}^2 \right) \quad (7)$$

$$A = \frac{8\rho(\pi\lambda)^{3/2}}{T^{3/2}} \quad (8)$$

where $\lambda = \hbar^2/2m$.

Under the assumptions of the impulse approximation, the classical Compton profile can be calculated from ref. 21–23,

$$J_{\mathrm{C}}(y) = (2\pi\sigma^2)^{-1/2} \exp\left(-\frac{y^2}{2\sigma^2} \right) \quad (9)$$

where σ is obtained by means of the kinetic energy,[21–23]

$$\langle K \rangle = \frac{3}{2} \frac{(\hbar\sigma)^2}{m} \quad (10)$$

Clearly, in the zero-density limit, eqn (4)–(6) are reduced to their classical counterparts, *i.e.* eqn (7)–(10).

The evolution of the system has been performed using a combination of bead-per-bead sampling, the bisection method, and displacements of the centroid of each polymer chain.[21–23] The acceptance of the bead-per-bead sampling was set as equal to 10%. Each simulation consisted of 4×10^7 Monte Carlo steps, of which the first 1.5×10^7 were discarded in order to guarantee equilibration. The stability of the results was confirmed by additional longer runs of 6×10^7 Monte Carlo steps, with the equilibrium averages for ^{4}He fully reproducible.

II.2 Feynman–Hibbs effective potentials

All Monte Carlo (MC) simulations have been performed in the canonical (N,V,T) ensemble. The interaction potential between ^{4}He atoms was also HFD-B2 He(4).[28] In total, we have performed two different kinds of MC simulations. First, we have done a classical simulation. Secondly, we have done two kinds of simulations using quantum-corrected versions of the interaction potential. These quantum corrections have been introduced by means of the second-order and fourth-order Feynman–Hibbs effective potentials, respectively,[12–15,25,26]

$$W_{\mathrm{FH}}(r) = \left\{ V(r) + \frac{\beta\hbar^2}{24\mu} \left(V''(r) + \frac{2V'(r)}{r} \right) \right\} \Theta(r_{\mathrm{cut}} - r) \quad (11)$$

$$W_{\mathrm{FH}}(r) = \left\{ V(r) + \frac{\beta\hbar^2}{24\mu} \left(V''(r) + \frac{2V'(r)}{r} \right) + \frac{\beta^2\hbar^4}{1152\mu^2} \left(\frac{15V'(r)}{r^3} + \frac{4V'''(r)}{r} + V''''(r) \right) \right\} \Theta(r_{\mathrm{cut}} - r) \quad (12)$$

where the prime, double prime, *etc.* denote the first, second, and higher order derivatives of the HFD-B2 He(4) classical potential with respect to r, $\mu = m/2$ is the reduced mass of a pair of interacting ^{4}He atoms, r_{cut} is the intermolecular cut-off distance and Θ is the Heaviside function. The number of atoms used in all MC simulations has ranged from 64 up to 300, using higher numbers for systems with higher densities. The intermolecular cut-off distance was set as equal to $5\sigma_{\mathrm{ff}}$ ($\sigma_{\mathrm{ff}} = 2.556$ Å). We performed a series of simulations for the longer cut-off distance of $7\sigma_{\mathrm{ff}}$. The computed static and thermodynamic properties of ^{4}He at the operating conditions were within the error of molecular simulations for both intermolecular cut-off distances. Each simulation consisted of 4×10^7 Monte Carlo steps, of which the first 1.5×10^7 were discarded in order to guarantee equilibration. The stability of the results was confirmed by additional longer runs of 6×10^7 Monte Carlo steps, with the equilibrium averages for ^{4}He fully reproducible.

III. Results and discussions

Before we consider the limitations of the semiclassical FH effective potentials, we discuss the PIMC results in close relation to the experimental measurements. In Fig. 1, we present the variation of kinetic energy of ^{4}He *versus* the number of beads quantizing ^{4}He atoms. Statistical uncertainties in all plots are omitted since the error bars are smaller than symbol size. The convergence of the kinetic energy is achieved for $P = 32$. In Fig. 2 we show the variation of density of ^{4}He over the pressure range up to 2.5 MPa. Despite the fact that ^{4}He above the λ transition can be treated as a Boltzmann fluid, it still exhibits some of the hallmarks of a quantum fluid. The departure from the classical regime as the temperature lowers can be explained with the delocalization of the ^{4}He atoms. In the PIMC formalism, this delocalization is represented by the swelling of the polymer ring.[27] We found that in the explored region of the ^{4}He phase diagram, the average gyration radius of polymer rings does not depend on pressure, *i.e.* $\langle R_g \rangle = 0.5$ Å, where $\langle R_g \rangle \equiv \left\langle (1/P) \sum_{\alpha=1}^{P} \left| \boldsymbol{r}_i^{(\alpha)} - \boldsymbol{R}_{\mathrm{CM},i} \right| \right\rangle$ and $\boldsymbol{R}_{\mathrm{CM},i}$ denotes the centroid position of the ith closed polymer chain. As expected, $R_g \cong \lambda/2$, where $\lambda \equiv (\beta\hbar^2/m)^{1/2} = 1.0$ Å for free ^{4}He at 10 K. Further, the volume of a classical ^{4}He atom is approximately $(4/3)\pi(1.278\ \text{Å})^3 = 8.7\ \text{Å}^3$, whereas the effective volume of a polymer ring quantizing a ^{4}He atom at 10 K and pressures up to 2.5 MPa computed from Monte Carlo integration is around 13.9 Å^3. Quantum delocalization increases the effective volume of the ^{4}He atom by approximately 60% (see movie 1 in ESI†). At very low densities, the mean kinetic energy values estimated by our PIMC simulations approach the classical limit, *i.e.* $K \to (3/2)k_BT$. Moreover, we observe a linear increase in the mean kinetic energy with increasing helium density. This linear dependence derives from the low-density range of ^{4}He studied here. At pressures over 0.5 MPa we observe a deviation of the classical equation of state from the experimental data. The linear variation of the mean kinetic energy with density, as well as the fact that the mean quantum kinetic energy of ^{4}He is *ca.* 48% larger than its classical counterpart at 2.5 MPa, suggest that our quantum fluid can be treated as a classical one at higher effective temperatures. Indeed, the momentum distributions of ^{4}He at 10 K, computed from the PIMC simulations, show a gradual modification of the width of the Maxwellian, depending on density. However, in the regime explored, quantum effects were not strong enough to deviate the momentum distribution from a Gaussian one, as it can be seen in Fig. 3. Therefore, we are allowed to fit the true quantum momentum distribution with a classical one computed at a higher effective temperature, as is displayed in Fig. 3. The effective temperature is obtained from $T_{\mathrm{eff}} = \langle K \rangle (2/3)k_B^{-1}$, where $\langle K \rangle$ is estimated from a PIMC simulation.

Now, we pay attention to the description of the experimental and PIMC results by semiclassical FH effective potentials. Note that our PIMC simulations correctly reproduce the thermodynamic and static properties of ^{4}He at the studied operating conditions. Moreover, in the considered range of the ^{4}He phase diagram, classical ^{4}He fluid (*i.e.* the limit of the infinite dilution) gradually transforms to a quantum one with increasing fluid pressure. That is why our model quantum fluid is perfect for the exploring of the limitations of the semiclassical FH effective potentials. If quantum effects are completely neglected, a strong attraction between classical ^{4}He atoms appears and an artificial phase transition above the critical point of ^{4}He is observed, as it is shown in Fig. 2. Interestingly, the low-order semiclassical FH quantum correction (second- or fourth-order) introduced to the classical HFD-B2 He(4) potential in the MC simulations produce only a slight improvement of the description of the equation of state,

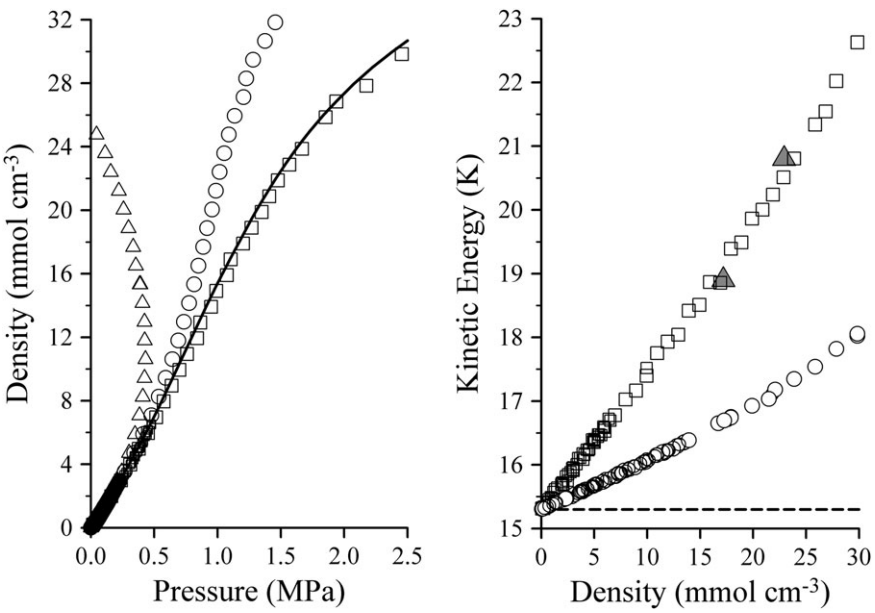

Fig. 2 Equation of state (left panel) and mean kinetic energy of ^{4}He (right panel) as a function of density at $T = 10$ K. Experimental data—solid line, classical MC simulations—open triangles, low-order semiclassical FH effective potential—open circles, PIMC simulations—open squares. Additionally, filled triangles on the right panel are taken from deep inelastic scattering experiments at high momentum transfers.[24]

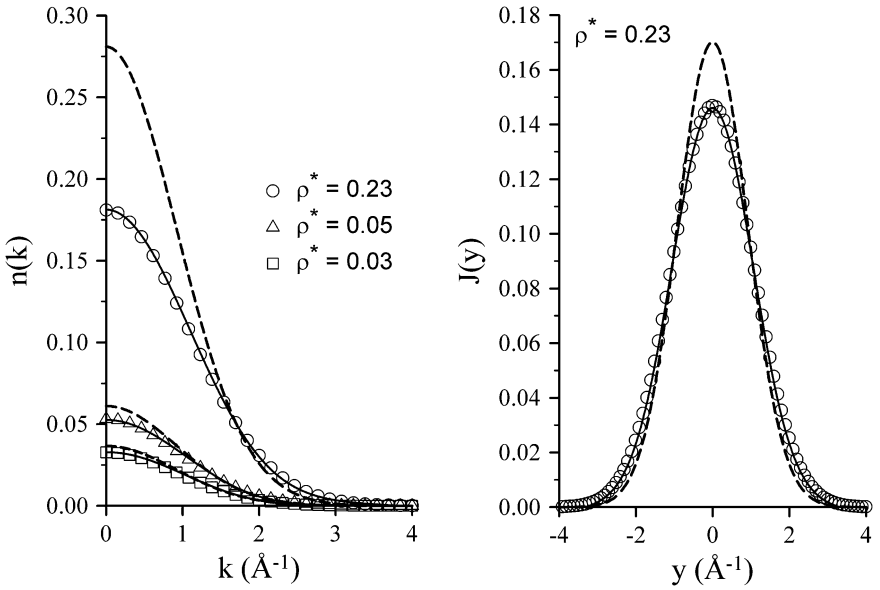

Fig. 3 Momentum distributions (left panel) and Compton profiles (right panel) computed from PIMC (solid lines), classical theory at $T = 10$ K (dotted lines) and classical theory at higher effective temperatures $T_{\text{eff}} = \langle K \rangle (2/3) k_{\text{B}}^{-1}$ (symbols), where $\langle K \rangle$ was computed from PIMC.

compared to purely classical theory. As can be seen in Fig. 2, above 0.7 MPa the semiclassical FH effective potentials gradually deviate from the experimental data. As we found from Fig. 2, this is a consequence of an underestimation of the mean kinetic energy. We found that semiclassical FH effective potentials reproduce the experimental densities of ^{4}He at 10 K for $\Lambda/a < 0.45$ ($\Lambda \equiv h/(2\pi m k_{\text{B}} T)^{1/2} = 2.73$ Å denotes the thermal de Broglie wavelength, $a = \rho^{-1/3}$ is the mean nearest-neighbor distance in the fluid and ρ denotes fluid density). Furthermore, we show that semiclassical FH effective potentials poorly reproduce the mean kinetic energy of ^{4}He at 10 K. And so, the mean kinetic energy computed from PIMC is reproduced by semiclassical FH potentials in a very limited range of fluid densities, *i.e.* $\Lambda/a < 0.17$. The density of *para*-H_2 adsorbed in carbon nanotubes and other nanoporous materials at cryogenic temperatures reached 50 mmol cm^{-3} (see ref. 10). Following the current study, we predict that semiclassical FH effective potentials give reliable estimations of this *para*-H_2 density at temperatures above 72 K (*i.e.* $\Lambda/a < 0.45$), whereas to reproduce the mean kinetic energy of dense liquid-like *para*-H_2 the temperature should exceed 510 K (*i.e.*, $\Lambda/a < 0.17$). This simple example shows that semiclassical FH effective potentials are poor approximations of liquid-like quantum liquids adsorbed in nanoporous materials at cryogenic temperatures. Thus, our simulation results seem to be particularly interesting for some fundamental problems of industrial importance. For example, the storage of hydrogen, neon and xenon at cryogenic temperatures, the transport of molecular hydrogen/deuterium in metal-hybrids, porous bodies, and alloys at cryogenic temperatures.

IV. Conclusions

We studied the applicability of the semiclassical Feynman and Hibbs (FH) (second-order or fourth-order) effective potentials to the description of the thermodynamic properties of quantum fluids at finite temperatures. We selected low-density ^{4}He at 10 K as our model quantum fluid. With PIMC, we obtained the experimental equation of state, the mean kinetic energy, the density matrix and the momentum distribution of this system at low densities. We showed that our PIMC results are in full agreement with static and thermodynamic properties of low-density ^{4}He at 10 K measured experimentally. Finally, we explored the limitations of the semiclassical FH effective potentials during the computation of the thermodynamic properties of quantum fluids at finite temperatures. We found that to reproduce the experimental density of quantum fluids by semiclassical FH effective potentials the reduced thermal de Broglie wavelength should fulfil the following condition: $\Lambda/a < 0.45$. In contrast, the mean kinetic energy can be only reproduced by these semiclassical potentials for $\Lambda/a < 0.17$. Our simulation results shine new light on the *ad hoc* application of the semiclassical FH effective potentials for the study of dense quantum fluids adsorbed in nanoporous materials.

Acknowledgements

P.K. gratefully acknowledges Prof. J. Doll, Dr Thanh X. Nguyen and Dr D. Colognesi for fruitful correspondences and suggestions on the content of the current paper. P.K. also acknowledges the Royal Melbourne Institute of Technology for a postdoctoral fellowship (Academic Level B, 2008–2010). P.A.G. and A.P.T. acknowledge the use of the computer cluster at Poznan Supercomputing and Networking Centre, as well as the Information and Communication Technology Centre of the Nicolaus Copernicus University (Torun, Poland).

References

1 L. Schlapbach and A. Züttel, *Nature*, 2001, **414**, 353.
2 H. Tanaka, H. Kanoh, M. Yudasaka, S. Iijima and K. Kaneko, *J. Am. Chem. Soc.*, 2005, **127**, 7511.

3 Q. Wang, S. R. Challa, D. Sholl and J. K. Johnson, *Phys. Rev. Lett*., 1999, **82**, 956.
4 Y. Hattori, H. Tanaka, F. Okino, H. Touhara, Y. Nakahigashi, S. Utsumi, H. Kanoh and K. Kaneko, *J. Phys. Chem. B*, 2006, **110**, 9764.
5 P. Kowalczyk, R. Holyst, M. Terrones and H. Terrones, *Phys. Chem. Chem. Phys*., 2007, **9**, 1786.
6 P. Kowalczyk, P. A. Gauden, A. P. Terzyk and S. K. Bhatia, *Langmuir*, 2007, **23**, 3666.
7 P. Kowalczyk, P. A. Gauden, A. P. Terzyk and S. Furmaniak, *J. Phys.: Condens. Matter*, 2009, **21**, 144210.
8 S. R. Challa, D. Sholl and J. K. Johnson, *Phys. Rev. B: Condens. Matter Mater. Phys*., 2001, **63**, 245419.
9 S. R. Challa, D. Sholl and J. K. Johnson, *J. Chem. Phys*., 2002, **116**, 814.
10 P. Kowalczyk, P. A. Gauden and A. P. Terzyk, *J. Phys. Chem. B*, 2008, **112**, 8275.
11 Q. Xu, D. Liu, Q. Yang and Ch Zhong, *Mol. Simul*., 2009, **35**, 748.
12 A. V. A. Kumar, H. Jobic and S. K. Bhatia, *Adsorption*, 2007, **13**, 501.
13 A. V. A. Kumar and S. K. Bhatia, *Phys. Rev. Lett*., 2005, **95**, 245901.
14 L. M. Sesé, *Mol. Phys*., 1994, **81**, 1297.
15 L. M. Sesé, *Mol. Phys*., 1995, **85**, 931.
16 S. W. Van Sciver, *Helium Cryogenics*, Plenum Press, New York, 1986.
17 D. M. Ceperley, *Rev. Mod. Phys*., 1995, **67**, 279.
18 A. Nakayama and N. Makri, *Proc. Natl. Acad. Sci. U. S. A*., 2005, **102**, 4230.
19 D. M. Ceperley, *Rev. Mod. Phys*., 1999, **71**, S438.
20 E. Rabani, G. Krilov, D. R. Reichman and B. J. Berne, *J. Chem. Phys*., 2005, **123**, 184506.
21 C. M. Ceperley and E. L. Pollock, *Can. J. Phys*., 1987, **65**, 1416.
22 L. Brualla, J. Boronat and J. Casulleras, *J. Low Temp. Phys*., 2002, **126**, 1547.
23 F. Mazzanti, J. Boronat and A. Polls, *Phys. Rev. B: Condens. Matter Mater. Phys*., 1996, **53**, 5661.
24 D. Colognesi, C. Andreani and R. Senesi, *Europhys. Lett*., 2000, **50**, 202.
25 R. P. Feynman and A. Hibbs, *Quantum Mechanics and Path Integrals*, McGraw- Hill, New York, 1965.
26 R. P. Feynman, *Statistical Mechanics*, Benjamin, New York, 1972.
27 K. Binder and D. W. Heermann, *Monte Carlo Simulation in Statistical Physics*, Springer-Verlag, Berlin, 2002.
28 R. A. Aziz, M. J. Slaman, A. Koide, A. R. Allnatt and W. J. Meath, *Mol. Phys*., 1992, **77**, 321.
29 E. Rabani and D. R. Reichman, *Annu. Rev. Phys. Chem*., 2005, **56**, 157.
30 E. Gallicchio and B. J. Berne, *J. Chem. Phys*., 1994, **101**, 9909.
31 D. R. Reichman and E. Rabani, *Phys. Rev. Lett*., 2001, **87**, 265702.
32 E. Rabani and D. R. Reichman, *J. Chem. Phys*., 2002, **116**, 6271.
33 D. R. Reichman and E. Rabani, *J. Chem. Phys*., 2002, **116**, 6279.
34 E. Rabani and D. R. Reichman, *Europhys. Lett*., 2002, **60**, 656.
35 T. D. Hone, P. J. Rossky and G. A. Voth, *J. Chem. Phys*., 2006, **124**, 154103.
36 J. A. Poulsen, G. Nyman and P. J. Rossky, *J. Chem. Theory Comput*., 2006, **2**, 1482.